Inorganica Chimica Acta 436 (2015) 16–22

Contents lists available at ScienceDirect

Inorganica Chimica Acta

journal homepage: www.elsevier.com/locate/ica

Biofilm inhibition by a new Mn(II) complex with sulfamethoxazole: Synthesis, spectroscopic characterization and crystal structure

Alejandro Di Santo [a], Diego M. Gil [b,*], Fernando Pomiro [c], Oscar E. Piro [d,1], Gustavo A. Echeverría [d,1], Mario Arena [e,1], Constanza Luciardi [e], Raúl E. Carbonio [c,1], Aída Ben Altabef [a,*,1]

[a] INQUINOA, CONICET, Instituto de Química Física, Facultad de Bioquímica, Química y Farmacia, Universidad Nacional de Tucumán, San Lorenzo 456, T4000CAN Tucumán, Argentina
[b] Instituto de Química Física, Facultad de Bioquímica, Química y Farmacia, Universidad Nacional de Tucumán, San Lorenzo 456, T4000CAN Tucumán, Argentina
[c] INFIQC (CONICET-Universidad Nacional de Córdoba), Departamento de Fisicoquímica, Facultad de Ciencias Químicas, Universidad Nacional de Córdoba, Ciudad Universitaria, X5000HUA Córdoba, Argentina
[d] Departamento de Física, Facultad de Ciencias Exactas, Universidad Nacional de La Plata and Institute IFLP (CONICET, CCT-La Plata), C. C. 67, 1900 La Plata, Argentina
[e] INQUINOA, CONICET and Facultad de Bioquímica, Química y Farmacia UNT, Ayacucho 471, T4000INI Tucumán, Argentina

ARTICLE INFO

Article history:
Received 7 April 2015
Received in revised form 19 June 2015
Accepted 10 July 2015
Available online 27 July 2015

Keywords:
Sulfa drugs metal complexes
Manganese complexes
X-ray crystal structure
IR and Raman spectroscopy
Antibacterial activity
Biofilm formation

ABSTRACT

The reaction in alkaline aqueous solution between sulfamethoxazole (SMX) and manganese (II) chloride produces colorless crystals with formula $[Mn(H_2O)_6]_{0.5}[Mn(SMX)_3]$, which was characterized by UV–Vis, IR and Raman spectroscopy and thermal analysis. The crystal structure of $[Mn(H_2O)_6]_{0.5}[Mn(SMX)_3]$ complex has been solved by X-ray diffraction methods. It crystallizes in the cubic *Pa*-3 space group with $a = 19.5476(1)$ Å, and $Z = 8$ molecules per unit cell. $[Mn(SMX)_3]^-$ complex is at a crystallographic special position of C_3 symmetry with the Mn(II) ion *cis*-coordinated to three equivalent sulfamethoxazole molecules acting as bidentate ligands in a propeller-like conformation. $[Mn(H_2O)_6]^{2+}$ hydrate ion is at crystal special position of S_6 symmetry with the metal in an almost perfect octahedral coordination with six water molecules. At 100 μg/mL $Mn(H_2O)_6]_{0.5}[Mn(SMX)_3]$ and SMX, inhibited the *Staphylococcus aureus* biofilm formation by 92% and 54%, respectively. However, at the same concentration $Mn(H_2O)_6]_{0.5}[Mn(SMX)_3]$ and SMX inhibited the planktonic bacterial growth by 52% and 81%, respectively. The Mn(II) complex inhibited the biofilm formation in values higher than 35% at the concentration 0.5 μg/mL. These results suggest that the metal complex $[Mn(H_2O)_6]_{0.5}[Mn(SMX)_3]$ is a good candidate for the development of new antimicrobial agent acting in part as bactericidal but mainly as antipathogenic agent.

1. Introduction

Sulfonamides were the first effective chemoterapeutic agents employed systematically for the prevention and cure of bacterial infections in humans. They are the drugs of choice for the treatment of chancroid, nocardiosis and acute urinary tract infections caused by several microorganisms including *Escherichia coli* and *Proteus mirabilis*. These substances can be used combined with other drugs in the treatment of otitis, meningitis, toxoplasmosis, recurrent and chronic urinary tract infections and in diarrhea, among other diseases [1–3]. Sulfonamides were also used in a variety of applications including antitumor agents [4], diuretics [5], carbonic anhydrase inhibitors [6], hypoglycaemic agents [7], and thyroid and protease inhibitors [8,9]. Recently, it was reported the presence of pathogens with sulfonamide-resistance genes in drinking water [10].

However, all the above-mentioned studies were carried out considering the bacteria as unicellular life forms. Direct observation of a wide variety of natural habitats has established that the 99% of microbes persist attached to surfaces within a structured biofilm ecosystem and not as free-floating organisms [11]. Today it is well-known the prevalence of biofilms in chronic infections and on medical implants. Bacteria that form biofilms can withstand host immune responses and are much more resistant to antibiotics than their counterpart planktonic bacteria. This effect is due to protective features of the film such as impedance against diffusion and favorable environment within the film [12].

* Corresponding authors at: Instituto de Química Física, Facultad de Bioquímica, Química y Farmacia, Universidad Nacional de Tucumán, San Lorenzo 456, T4000CAN San Miguel de Tucumán, Argentina. Tel.: +54 381 4311044; fax: +54 381 4248169.
E-mail addresses: dmgil@fbqf.unt.edu.ar (D.M. Gil), altabef@fbqf.unt.edu.ar (A.B. Altabef).
[1] Member of the Research Career of CONICET.

http://dx.doi.org/10.1016/j.ica.2015.07.024
0020-1693/

Therefore, infections with biofilm forming bacteria are persistent and difficult to treat with antibiotics. Bacteria in biofilms survive exposure to concentrations of antibiotics 1000-fold greater than the one that are lethal when the free cells are in suspension [12]. For this reason, the development of anti-infective compounds, which are active not only against planktonic microorganisms but mainly also against biofilms represents an imperative goal [13].

The chemistry of metal complexes with heterocyclic compounds containing nitrogen, sulfur, and/or oxygen as ligand atoms has attracted increasing attention. It is well-known that metal-based therapeutics for treatment of many ailments have gained much attention during the past decade. The ability of metal ions to bind *in vivo* with proteins and peptides is an important feature of metal-based drugs. Simple and N-substituted sulfonamides have attracted much attention in this context. The development of new metal complexes with sulfonamides is an important field of research, considering that one can combine the specific antibacterial activities of the sulfonamides and the multi-targeting antimicrobial activities of the metal ions. In many cases, the metal complex exhibits a better activity than the free ligand at the same experimental conditions [14]. In particular, silver sulfonamides compounds have proved to be effective topical antimicrobial agents, especially Ag-Sulfadiazine (Ag-SDZ) used in burn therapy [15]. Ag-SDZ has shown to be insoluble in water and in other common organic solvents, which limits its application in medicine.

Sulfamethoxazole (SMX) was part of the second generation of sulfonamides (see Scheme 1) and it is used in a synergistic combination with trimethropim. SMX is the drug most used to treat infections produced by *Pneumocystis pneumonia*, which is a form of pneumonia caused by a yeast-like fungus that affects patients with HIV [16]. There are also some metal complexes of sulfamethoxazole reported in the literature [17–26]. Two Cd(II) complexes of sulfamethoxazole were obtained and their crystal structures were reported [19,20]. In $[Cd(SMX)_2(CH_3OH)_2]$, the Cd(II) centers are linked through sulfamethoxazolate anions which alternate in their coordination with the isoxazolic N-atoms and the aromatic amino groups [19]. A similar structure was obtained for $[Cd(SMX)_2(L)_2]$ complexes (L = Dimethylformamide, dimethyl sulfoxide and pyridine) [20]. Mondelli et al. have reported the synthesis and structural characterization of $[Co(SMX)_2(H_2O)_2]\cdot H_2O$ complex, where Co(II) is in a slightly tetragonally distorted octahedron where the SMX molecules act as a head-to-tail bridges between two Co atoms forming polymeric chains [23]. Marques et al. have synthesized Au(I) and Ag(I) complexes with SMX as ligand. Both complexes present a linear geometry and the SMX bind to Au and Ag through the N of the sulfonamide group [22]. The antibacterial activities of both complexes were determined and the gold complex showed greater activity against *E. coli* and *Staphylococcus aureus* than the silver one [22]. However, there are not information about the effect of sulfamethoxazole complex against bacterial biofilm.

In the present contribution we report the synthesis and spectroscopic characterization of a new Mn(II) complex with sulfamethoxazole as ligand with formula $[Mn(H_2O)_6]_{0.5}[Mn(SMX)_3]$. The crystal structure was determined by single-crystal X-ray diffraction methods. To the best of our knowledge, no previous study on the anti-biofilm activity of sulfamethoxazole complex against *S. aureus*.

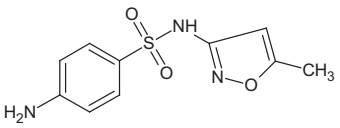

Scheme 1. Structure of sulfamethoxazole.

2. Experimental

2.1. Synthesis of $[Mn(H_2O)_6]_{0.5}[Mn(SMX)_3]$ complex

The Mn(II) complex with sulfamethoxazole was synthesized by mixing together aqueous solutions of the appropriate $MnCl_2\cdot 4H_2O$ (1 mmol) and sodium sulfamethoxazole (2 mmol) under continuous stirring at room temperature (RT). The precipitate formed was separated by filtration and the slow evaporation of the remaining solution gave suitable crystals for structural X-ray diffraction. The complex was soluble and stable in water, dimethylsulfoxide (DMSO) and dimethylformamide (DMF).

2.2. Crystallographic data and structure determination

The X-ray measurements were performed on an Oxford Xcalibur, Eos, Gemini CCD diffractometer with graphite-monochromated CuKα (λ = 1.54184 Å) radiation. X-ray diffraction intensities were collected (ω scans with θ and κ-offsets), integrated and scaled with CrysAlisPro [27] suite of programs. The unit cell parameters were obtained by least-squares refinement (based on the angular settings for all collected reflections with intensities larger than seven times the standard deviation of measurement errors) using CrysAlisPro. Data were corrected empirically for absorption employing the multi-scan method implemented in CrysAlisPro. The structure was solved by direct methods with SHELXS-97 program of the SHELX package [28] and the corresponding molecular model developed by alternated cycles of Fourier methods and full-matrix least-squares refinement with the program SHELXL-97 of the same package. All H-atoms were located in a Fourier difference map phased on the heavier atoms and refined at their found positions with isotropic displacement parameters. The methyl group converged to a staggered conformation. Crystal data, data collection procedure, structure determination methods and refinement results are summarized in Table 1. Crystallographic structural data have been deposited at the Cambridge Crystallographic Data Centre (CCDC). Any request to the CCDC for this material should quote the full literature citation and the reference number CCDC 1057060.

2.3. Physical measurements

The FTIR absorption spectrum of the solid state compound was recorded from KBr pellets in the 4000–400 cm^{-1} frequency range with a Perkin–Elmer GX1 Fourier Transform infrared instrument. The corresponding Raman dispersive spectrum was measured in the 3500–50 cm^{-1} interval with a Thermoscientific DXR Raman microscope. The Raman data were collected (at 5 cm^{-1} spectral resolution) using a diode-pump solid state laser of 532 nm wavelength, a con-focal aperture of 25 μm pinhole and 10x objective. The sample was placed on gold-coated sample slides. To achieve a sufficient signal to noise ratio, 30 spectral scans of 2 s each were accumulated during the measurements with the laser power maintained at 10 mW. UV–Vis measurements were recorded using quartz cells (10 mm optical path length) on a Beckman/DU 7500 spectrophotometer. For this purpose, a solution of 10^{-4} mol/L of the complex in DMSO was prepared. The spectrum was recorded between 800 and 200 nm. Calorimetric measurements were performed using a differential scanning calorimeter Perkin Elmer Pyris DSC 6. The experiments were carried out using 3.980 mg of powdered sample sealed in aluminum pans with a mechanical crimp. Temperature and heat flow calibrations were made with standard samples of indium by using its melting transition. Enthalpy changes associated with the dehydration of the sample in study (ΔH) was directly obtained from the DSC data by

Table 1
Crystal data and structure refinement results for $[Mn(H_2O)_6]_{0.5}$ $[Mn(SMX)_3]$.

Empirical formula	C_{30} H_{36} $Mn_{1.50}$ N_9 O_{12} S_3
Formula weight	893.27
T (K)	293(2)
λ (Å)	1.54184
Crystal system	cubic
Space group	*Pa*-3
Unit cell dimensions	
a (Å)	19.5476(1)
V (Å^3)	7469.31(7)
Z	8
D_{calc} (Mg/m^3)	1.589
Absorption coefficient (mm^{-1})	6.398
F(000)	3684
Crystal shape/color	Fragment/colorless
Crystal size (mm)	0.135 × 0.152 × 0.182
θ-range for data collection (°)	3.92–72.38
Index ranges	$-8 \leqslant h \leqslant 21$, $-11 \leqslant k \leqslant 21$, $-21 \leqslant l \leqslant 24$
Reflections collected	7074
Independent reflections (R_{int})	2441 (0.026)
Observed reflections [$I > 2\sigma(I)$]	2185
Completeness to θ = 72.38°	98.8%
Refinement method	Full-matrix least-squares on F^2
Data/restraints/parameters	2441/0/216
Goodness-of-fit (GOF) on F^2	1.070
Final R indices[a] [$I > 2\sigma(I)$]	R_1 = 0.0297, wR_2 = 0.0757
R indices (all data)	R_1 = 0.0346, wR_2 = 0.0791
Largest difference peak and hole (e Å^{-3})	0.306 and −0.332

[a] $R_1 = \Sigma||F_o| - |F_c||/\Sigma|F_o|$, $wR_2 = [\Sigma w(|F_o|^2 - |F_c|^2)^2/\Sigma w(|F_o|^2)^2]^{1/2}$.

integrating the anomalous peak in the baseline-subtracted curve. Thermo-gravimetric (TGA) and differential thermal analysis (DTA) measurements were performed with a Shimadzu DTG-60 thermo-balance in the temperature range from 25 to 800 °C at a heating rate of 5 °C/min under air flow (90 mL/min). Powder X-ray Diffraction (PXRD) pattern for the residue obtained by thermal decomposition of $[Mn(H2O)_6]_{0.5}[Mn(SMX)_3]$ was recorded at RT on a PANanalitycal X'Pert PRO diffractometer in Bragg–Brentano geometry with Cu Kα radiation.

2.4. Bacterial growth

Overnight cultures of *S. aureus* ATCC 6538 were diluted to reach an OD (0.125 ± 0.02) at 560 nm in Müeller Hilton (MH) medium. The diluted culture (190 μL) was then placed in each of the 96 wells of a microtitre polystyrene plate. Solutions containing 2, 1, 0.5, 0.2, 0.1, 0.02 and 0.01 mg/mL of SMX and Mn(II)-SMX DMSO/distilled water (1:1) were prepared separately and 10 μL of each was pipetted into the plastic microtitre plate wells individually (8 replicates). Control wells (8 replicates) contained the diluted culture (190 μL) and 10 μL of a solution of DMSO/water (1:1) in which the final concentration of DMSO is 2.5%. Medium control was prepared using sterile LB. Bacteria grew in LB medium at 37 °C and growth was detected as turbidity (560 nm) using a microtitre plate reader (Power Wave XS2, Biotek, VT, USA). The maximum level of DMSO to which the cells were exposed was 2.5%.

2.5. Biofilm formation assay

For biofilm quantification, a micro method based on a protocol previously reported was employed [29]. Biofilms formed after 24 h incubation of bacterial cultures prepared as described in the previous paragraph, were stained with 20 μL of an aqueous solution of crystal violet (0.1%, w/v) for 20 min. After washing with water, the liquid was discarded from the wells and the material that remained fixed to the polystyrene (containing bio-film) was washed with PBS (thrice). Crystal violet bound to biofilm was removed from each well employing 200 μL absolute ethanol during 30 min at 37 °C with shaking. Absorbance (560 nm) of ethanol solutions of crystal violet was determined using a microtitre plate reader (Power Wave XS2, Biotek, VT, USA).

3. Results and discussion

3.1. Crystal structure

The complex $[Mn(H_2O)_6]_{0.5}[Mn(SMX)_3]$ crystallizes in the cubic crystal system, space group *Pa*-3 (#205) with cell parameters $a = b = c$ = 19.5476(1) Å and V = 7469.31(7) Å^3. The unit cell accommodates eight formula units (Z = 8). Table 1 summarizes details for the crystal structure determination and refinement results. An ORTEP [30] plot of the title complex is shown in Fig. 1 and bond distances and angles around the Mn(II) ions are listed in Table 2. The $[Mn(SMX)_3]^-$ complex and the $[Mn(H_2O)_6]^{2+}$ hydrate ion are at crystal special positions of C_3 (3) and S_6 ($\bar{3}$) site symmetries, respectively. In the complex $[Mn(SMX)_3]^-$ the manganese ion is in a distorted octahedral environment, *cis*-coordinated to a sulfamethoxazolate molecule acting as bidentate ligand through its oxazolyl ring N-atom [d(Mn–N) = 2.225(2) Å] and one sulfoxide oxygen atom [d(Mn–O) = 2.244(1) Å] in a three blades propeller-like conformation. The ligand is folded such as to optimize the π–π interaction between the 4-amino benzene ring and the oxazolyl ring of a neighbor, symmetry related, ligand [ring planes separation of about 3.5 Å]. The metal in $[Mn(H_2O)_6]^{2+}$ is in an almost perfect octahedral coordination with water molecules nearly along the oxygen lone pair [d(Mn–Ow) = 2.171(2) Å].

Bond distances within the benzene ring of $[Mn(SMX)_3]^-$ complex are in the range 1.376(3)–1.395(3) Å, as expected for a resonant-bond structure. In the oxazolyl ring (see Fig. 1), C7–C8 distances [1.337(3) Å] is considerable shorter [in 0.077(3) Å] than C8–C9 length hence indicating formally double and single bonds for these links. The C(9)–N(2)–S(1) angle is 119.64° hence suggesting a sp^2 hybridization in accordance with the deprotonation of the sulfonamidic N atom. S1–N2, N2–C9, and C9–N3 bond lengths [1.568(2), 1.373(2), and 1.327(2)–Å] suggest π-delocalization along these bonds that promotes the near co-planarity observed for these links [S1–N2–C9–N3 torsion angle of 12.7(3)°]. As expected due to Mn–O1 ligand interaction, the sulfoxide S1=O1 bond distance [1.474(1) Å] is significant longer [in 0.027(1) Å] than S1=O2 length of the unbounded-to-metal group.

Neighboring complexes in the lattice are bridged by the water molecule through relatively strong and linear O1w–H1···N2′ and O1w–H2w···O2″ bonds [d(H1w···N2′) = 1.976 Å, ∠(O1w-H1w···N2′) = 174.3°; d(H2w···O2‴) = 2.120 Å, ∠(O1w–H2w···O2″) = 171.3°]. The complexes are also directly linked to each other through a weak and bent N1–H···O1 bonds [d(H1A···O1′) = 2.330 Å, ∠(N1–H1A∠O1′) = 138.6°; d(H1B···O1″) = 2.604 Å, ∠(N1–H1B···O1″) = 126.3°]. Further details of the H-bonding structure is provides as a Supplementary material (Table S5).

The coordination behavior of the sulfamethoxazolate anion in the complex differs from that exhibited in $[Zn(SMX)_2(py)_2(H_2O)_2]$ where the sulfamethoxazolate anion only acts as monodentate ligand through the isoxazole N-atom [24]. The sulfamethoxazolate complexes with general formula $[M(SMX)_2(H_2O)_2]\cdot H_2O$ (M = Co, Ni) are isostructural and they crystallize in the monoclinic system. In their crystal structure, the M(II) ions are six coordinated by two oxygen atoms from two coordinated water molecules, two N atoms from N-arylamine and two N atoms from N-sulfonamide [23,31]. A similar mode of coordination was found for $[Cd(SMX)_2(CH_3OH)_2]_n$ where the Cd atoms are coordinated by two isoxazole and two aniline N atoms (of four sulfamethoxazolate anions) besides two methanol molecules [19]. In the structure, the metal centers are

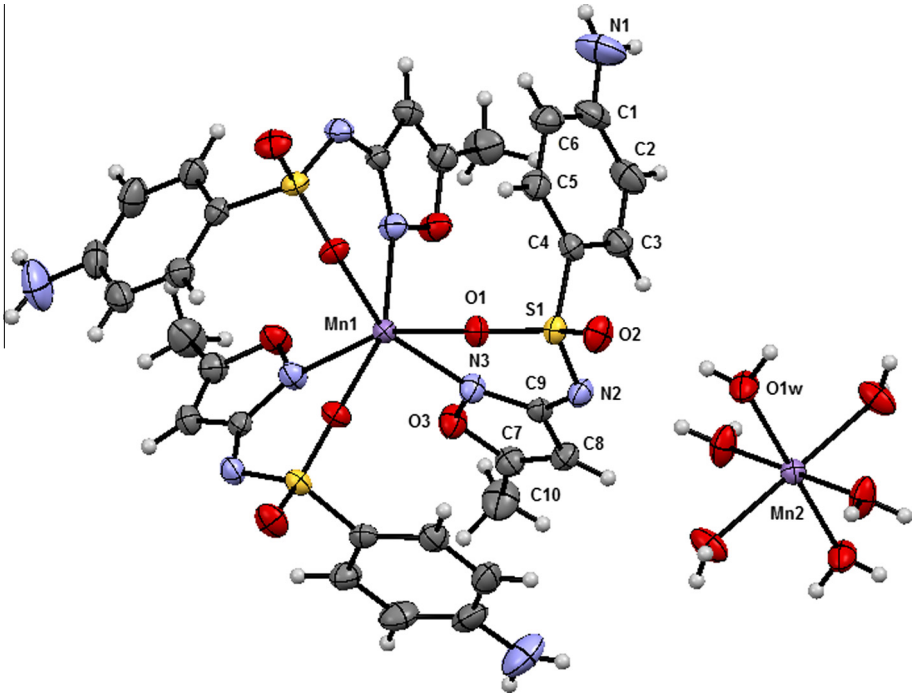

Fig. 1. Drawing of [Mn(H2O)6]½[Mn(SMX)3] complex showing the labeling of the non-H atoms and their displacement ellipsoids at the 30% probability level. Metal–ligand interactions are indicated by open bonds.

Table 2
Bond lengths [Å] and angles [°] around the metals in $[Mn(H_2O)_6]_{0.5}$ $[Mn(SMX)_3]$.

Mn(1)–N(3)	2.225(2)
Mn(1)–O(1)	2.244(1)
Mn(2)–O(1W)	2.171(2)
N(3)–Mn(1)–N(3)#1	96.13(5)
N(3)–Mn(1)–O(1)#2	157.60(5)
N(3)–Mn(1)–O(1)	77.24(5)
O(1)#2–Mn(1)–O(1)	83.96(5)
N(3)–Mn(1)–O(1)#1	105.78(5)
O(1W)–Mn(2)–O(1W)#3	88.21(7)
O(1W)–Mn(2)–O(1W)#4	91.79(7)

Symmetry transformations used to generate equivalent atoms: (#1) *y*, *z*, *x*; (#2) *z*, *x*, *y*; (#3) *y* + 1/2, *z*, −*x* + 1/2; (#4) −*y* + 1/2, −*z*, *x* − 1/2.

linked to each other through sulfamethozaxolate bridges forming a polymeric array. The polymeric structure observed for $[Cd(SMX)_2(CH_3OH)_2]_n$ is not usual in sulfonamides complexes.

3.2. Characterization of $[Mn(H_2O)_6]_{0.5}[Mn(SMX)_3]$

A comparative study of the IR and Raman spectra of the complex with that of the free ligand and those of the complexes of related ligands gives some positive information regarding the binding sites of sulfamethoxazole [25]. The IR spectrum of the metal complex $[Mn(H_2O)_6]_{0.5}[Mn(SMX)_3]$ taken in the 4000–400 cm^{-1} region are compared with those of the free ligand in Fig. 2. Fig. 3 shows the Raman spectra of Sulfamethoxazole and $[Mn(H_2O)_6]_{0.5}[Mn(SMX)_3]$ complex. The characteristic IR and Raman bands of the spectra and their corresponding assignment are shown in Table 3. The bands that appear between 3500 and 3400 cm^{-1} due to the NH_2 antisymmetric and symmetric vibrations are modified with respect to those of the free ligand. These modifications are most probably due to the hydrogen bonding between complexes involving the NH_2 and SO_2 groups (see Section 3.1). The weak band located at 3473 cm^{-1} and the medium-intensity band located at 3451 cm^{-1} in the IR spectrum of

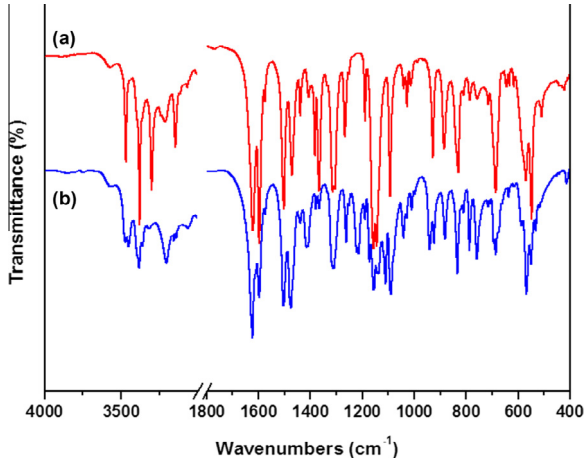

Fig. 2. IR spectra of: (a) Sulfamethoxazole ligand; (b) $[Mn(H_2O)_6]_{0.5}[Mn(SMX)_3]$.

the complex are assigned to the NH_2 antisymmetric stretching vibration. This band appears at 3068 cm^{-1} in the IR spectrum of the free ligand. The band located at 3381 cm^{-1} in the IR spectrum (3365 cm^{-1} in Raman) is assigned to the symmetric stretching mode of the NH_2 group. The IR band for the sulfonamidic N–H group in the free ligand is located at 3299 cm^{-1} and is absent in the spectrum of the complexes, a fact that confirms the deprotonation of the $-SO_2NH-$ moiety. The very strong band located at 1623 cm^{-1} in the IR spectrum of the complex (1624 cm^{-1} in Raman) is assigned to the NH_2 bending mode. The four typical vibrational modes of the sulfonyl group are detected in the free SMX and also in the complex. For SMX, the strong IR bands located at 1314 and 1305 cm^{-1} (1313 and 1304 cm^{-1} in Raman) are assigned to the SO_2 antisymmetric stretching mode. The IR bands at 1157 and 1145 cm^{-1} are assigned to the SO_2 symmetric stretching mode. Both bands show significant changes upon complexation as a consequence of coordination to the metal (see Fig. 1 and

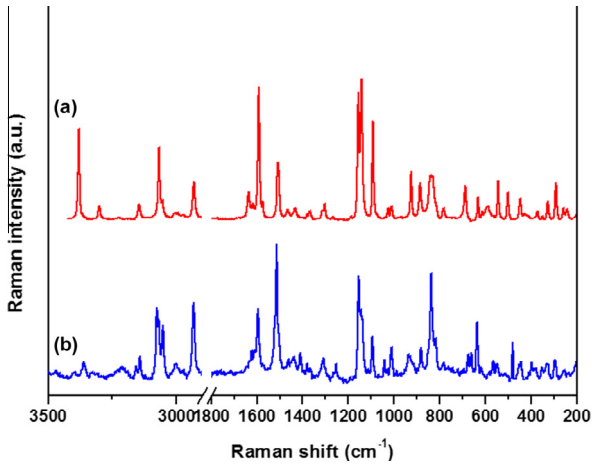

Fig. 3. Raman spectra of: (a) Sulfamethoxazole ligand; (b) $[Mn(H_2O)_6]_{0.5}$-$[Mn(SMX)_3]$.

discussion in Section 3). In the complex, the IR bands associated to the ν_a (SO_2) appear at 1222 and 1214 cm^{-1} and the bands corresponding to the ν_s (SO_2) are located at 1117 and 1109 cm^{-1}. The IR band corresponding to the SO_2 bending mode in the complex appears as a medium-intensity band at 550 cm^{-1}. The S-N stretching vibration of the complex is observed as a medium-intensity band in the IR spectrum at 940 cm^{-1} (938 cm^{-1} in Raman), while in the ligand this IR band appears at 928 cm^{-1} (926 cm^{-1} in Raman). The observed blue shift is in accordance with the shortening of the S–N bond length as observed in the solid state structure of the complex (see Table S1). The vibrational spectrum of isoxazole ring has been described by several authors [32,33]. Because of the rigidity of the five-membered ring, the spectrum cannot be interpreted in terms of localized vibrations. Similar to other complexes with isoxazole, in $[Mn(H_2O)_6]_{0.5}[Mn(SMX)_3]$ only three isoxazole bands showed significant shifts. The bands of unbonded SMX ligand at 3144, 1502 and 885 cm^{-1} shift to 3156, 1514 and 881 cm^{-1}, respectively, upon coordination. Most of the other shifts were small. The very weak band located at 445 cm^{-1} in the IR and Raman spectra and the weak IR band at 413 cm^{-1} are assigned to the Mn–O stretching mode. The band located at 398 cm^{-1} in the Raman spectrum is assigned to the $Mn–N_{isozaxole}$ stretching mode.

The UV–Vis spectrum of the complex in DMSO solution presents a maximum absorption attributable to the SMX ligand. The band located at around 250–260 nm is assigned to $\pi \rightarrow \pi^*$ transitions within the organic molecule while an intraligand band at 280–290 nm is related to the $\pi \rightarrow \pi^*$ transitions within the heterocyclic moieties. The band located at 410 nm is assigned to metal–ligand charge transfer. No d–d transition is expected for Mn(II) complexes.

The thermal behavior of $[Mn(H_2O)_6]_{0.5}[Mn(SMX)_3]$ has been studied using thermogravimetric (TG) and differential thermal (DTA) analysis from RT to 800 °C in air. TG and DTA curves for the thermal decomposition of the complex are shown in Fig. 4. The thermal decomposition of the complex takes place in three steps. The first one finishes at 216 °C and corresponds to the loss of the water molecules coordinated to the Mn(II) atom with a mass loss of 5.78% (theoretical value 6.05%). The DTA curve shows two endothermic peaks located at 170 and 202 °C assigned to the dehydration process. After the release of water, a complex degradation process of the remaining material is observed. As shown in Fig. 5, two consecutive TG steps are observed: the first one between 216 and 473 °C (with two weak exothermic peaks located at 270 and 458 °C in DTA) and the second one between 473 and 565 °C. For the last step, a very strong exothermic peak located at 528 °C is observed in the DTA curve. These peaks are attributed to the combustion of the organic ligand to produce Mn_3O_4 as final product. This substance was identified by PXRD measurements (See Fig. S1). The mass loss observed at 565 °C was 84.75% and it was

Table 3
Characteristic IR and Raman bands (cm^{-1}) in the spectra of sulfamethozaxole and $[Mn(H_2O)_6]_{0.5}[Mn(SMX)_3]$ complex.

Sulfamethoxazole		$[Mn(H_2O)_6]_{0.5}[Mn(SMX)_3]$		Assignment[b]
IR (solid)[a]	Raman (solid)	IR (solid)	Raman (solid)	
3068 m	–	3473 w	–	ν_a NH_2
–	–	3451 m	–	
3378 s	3380	3381 m	3365	ν_s NH_2
3299 s	3300	–	–	ν N–H (isoxazole ring)
–	–	3156 w	3157	ν C–H (isoxazole ring)
3144 m	3146	–	3143	
1622 vs	1620	1623 vs	1624	δ NH_2 + ν C–C (isoxazole ring)
1597 vs	1592	1597 m	1595	ν C=C (aromatic)
1502 s	1507	1503 s	1514	ν C–C (isoxazole ring)
1471 m	1469	1479 sh	–	ν C–C (isoxazole ring)
–	–	1475 m	1470	
1314 s	1313	1222 m	–	ν_a SO_2
1305 s	1304	1214 m	–	
1267 m	1267	1262 m	1263	ν C–N
1157 vs	1156	1117 sh	1116	ν_s SO_2
1145 vs	1143	1111 m	1109	
1093 s	1093	1089	1095	δ C–H (aromatic)
928 m	926	940 m	938	ν S–N
885 m	886	881 m	881	γ C–H (isoxazole ring)
829 m	830	833 m	837	δ C–H
686 s	688	686 m	–	ν C–S
570 m	–	568 s	–	ω SO_2
548 s	545	550 m	551	δ SO_2
509 w	501	–	480	ρ SO_2
–	–	445 vw	445	ν Mn–O
–	–	413 w	–	ν Mn–O
–	–	–	398	ν Mn–N (isoxazole ring)

[a] sh, shoulder; s, strong; w, weak; m, medium; v, very.
[b] ν: stretching, δ: in-plane deformation, γ: out-of-plane deformation, ρ: rocking, ω: wagging, $\tau\omega$: twisting modes.

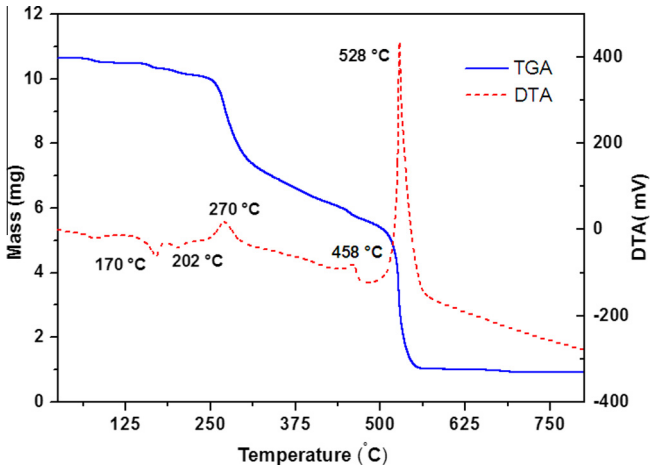

Fig. 4. TGA and DTA curves for the thermal decomposition of $[Mn(H_2O)_6]_{0.5}[Mn(SMX)_3]$ in air.

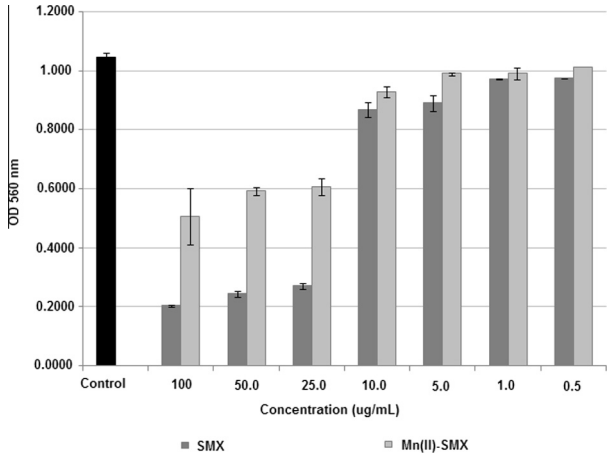

Fig. 5. Effect of different concentrations of SMX and $[Mn(H_2O)_6]_{0.5}[Mn(SMX)_3]$ on *S. aureus* ATCC 6738 growth. The error bars indicate standard deviation (SD).

in agreement with the theoretical value (81.14%) calculated for the formation of Mn_3O_4 from the complex. Fig. S2 shows the DSC curve for $[Mn(H_2O)_6]_{0.5}[Mn(SMX)_3]$. This study was performed to look for possible structural transitions and to evaluate the thermodynamic parameters associated to the dehydration process of the compound. The DSC scan clearly shows an endothermic peak located at 174 °C. This transition is attributed to the loss of water molecules coordinated to Mn(II). It is in agreement with the results observed by TG and DT analyses. The estimated enthalpy variation (ΔH) for the dehydration process is 39.97 kJ mol^{-1}. As shown in Fig. S2, the decomposition of the sample takes place at around 250 °C, in accord with the thermogravimetric analysis.

3.3. Antibacterial effect

The results of antibacterial activities of the ligand and metal complex are shown in Fig. 5. SMX and Mn(II)-SMX complexes caused considerable bacterial growth inhibition compared to the control. At 100 μg/mL the inhibition was 81 and 52%, respectively. The decreased on the bacterial growth was directly proportional to complex concentration. At 1 μg/mL the bacterial growth inhibition was 7% and 5% by SMX and Mn(II)-SMX, respectively.

Manganese (II) is a required cofactor for metabolic processes that facilitate staphylococcal growth [34]. On the other hand, the use of Mn(II) complexes by bacteria, to provide a basal level of protection against reactive oxygen species, as well as the existence of Mn(II) permeases, has been confirmed in *S. aureus* [35]. The presence of Mn appears to diminish the growth inhibitory power of SMX against free-living cells. Our results are in agreement with previous studies that found a higher *S. aureus* bacterial growth inhibition with complexes of coumarin without Mn as compared with the same complexes with Mn [36]. In contrast, the antibacterial effect of Mn(II)-Tetraphenyl porphyrin (TPP), ebselen–porphyrin conjugate, and its Mn(II) complex towards *S. aureus* growth indicates a higher inhibition in presence of Mn. However, the concentration that inhibited 50% the bacterial growth was 100 μg/mL [37]. This values were similar to those obtained at the same concentration in presence of Mn(II), but lower than the obtained with the complex without Mn(II). The enhancement in antibacterial activity of the metal complexes can be explained based on the chelation theory [38]. Upon chelation to a metal ion, the ligand polarity will be reduced largely due to the overlap of ligand orbital and the partial sharing of positive charge of the metal ion with donor groups. Futhermore, the chelation process increases the delocalization of the π electrons over the whole chelate ring, which results in an increase in the lipophilicity of the metal complexes. Consequently, these complexes can easily penetrate into the lipid membranes and block the metal binding sites of microorganism enzymes [39]. These metal complexes also affect the cell respiration process hence blocking the synthesis of proteins, which in turn further restrict the growth of the organism [39]. Apart from this, other factors such as solubility, conductivity and dipole moment, as influenced by the presence of metal ions, may also be among the possible reasons causing enhancement of the antibacterial activity of the metal complexes as compared to the un-complexed compounds [40].

3.4. Biofilm formation

The experimental results for the biofilm formation in presence of SMX and Mn(II)–SMX at different concentrations is presented in Fig. 6. The biofilm formed after 24 h incubation was inhibited to 54% and 92% levels, by the presence of 100 μg/mL of SMX and Mn(II)–SMX, respectively. To inhibits 50% of biofilm formation (IC50) with Mn(II)–SMX it is necessary a concentration of only 7.83 μM. Since one of the strongest biofilm inhibition (two small

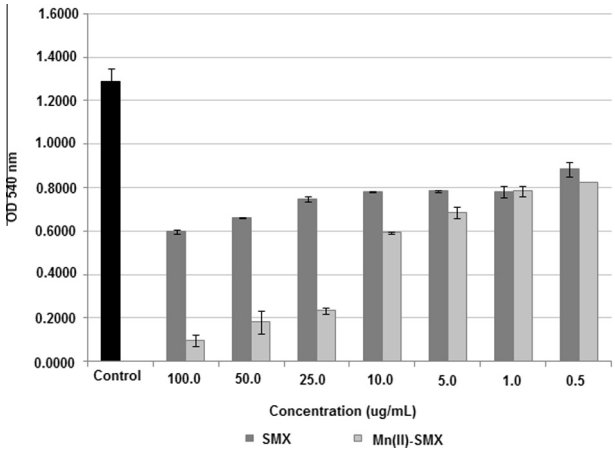

Fig. 6. Effect of different concentrations of SMX and $[Mn(H_2O)_6]_{0.5}[Mn(SMX)_3]$ on *S. aureus* ATCC 6738 biofilm formation. The error bars indicate standard deviation (SD).

synthesized compound CCG_203592 and CCG-205363) cause 50% inhibition at 2.42 and 6.96 μM, the effects of Mn(II)–SMX might be considered as a good inhibitor [41]. This result suggests an effect on the mechanism involved in biofilm formation, quorum sensing, more than an antibiotic property. Our results indicate that Mn(II)–SMX is a good candidate for the development of new anti-biofilm agent.

In the results published by Wunder et al., it was evaluated the sorption of antibiotics to biofilm, including sulfamethoxazole (SMX), ciprofloxacin (CIP), and erythromycin (ERY). CIP and ERY compounds have the greatest biofilm partition coefficient. It appears that speciation (i.e. charge) and antibiotic molecular size are important factors in explaining their sorption to typically negatively charged biofilm. SMX is neutral to negatively charged at circumneutral pH while CIP and ERY are both positively charged [42]. The higher activity of Mn(II) complex could be explained in terms the metal positive charge. On the other hand, for *S. aureus* biofilm formation is necessary the expression of collagen adhesin, a collagen-binding protein, from the cell surface of *S. aureus* [43]. For these adhesions low Mn concentration are required [44].

4. Conclusions

The metal complex $[Mn(H_2O)_6]_{0.5}[Mn(SMX)_3]$ was synthesized and characterized by IR, Raman, UV–Vis and thermal analysis. The solid state structure of the complex was solved by single-crystal X-ray diffraction methods. In $[Mn(SMX)_3]^-$ complex, the manganese(II) ion is coordinated by three SMX molecules acting as bidentate ligand in a propeller-like conformation. The $[Mn(H_2O)_6]^{2+}$ hydrated ion, the Mn(II) metal is an almost perfect octahedral coordination with water molecules. Vibrational IR and Raman spectroscopic data reveal that the SMX ligand coordinate through its oxazolyl ring N-atom and one sulfoxide oxygen atom.

The thermal decomposition of the complex takes place in three steps. The first one corresponds to the loss of water molecules of the $[Mn(H_2O)_6]^{2+}$ ion. The decomposition of the complex proceeds in two consecutive steps related to the combustion of the organic ligand to produce Mn_3O_4 as final product.

The antibiofilm property of SMX against of the human pathogen *S. aureus* increased significantly due to addition of Mn to the complex. Taken into account the importance of biofilm in microbial resistance to antibiotics and disinfectants, the new complex is a good candidate for the development of new antimicrobial agent acting in part as bactericidal but mainly as anti-pathogenic pharmaceutical.

Acknowledgements

This work was supported by CIUNT (D542), CONICET (PIP 0205 and PIP 1529) and by ANPCyT (PICT 2013-0697, PME06 2804, and PICT06 2315) of Argentina. O.E.P. and G.A.E. are Research Fellows of CONICET. A.D.S. thanks Consejo Interuniversitario Nacional (CIN) for a fellowship.

Appendix A. Supplementary material

CCDC 1057060 contains the supplementary crystallographic data for this paper. These data can be obtained free of charge from The Cambridge Crystallographic Data Centre via http://www.ccdc.cam.ac.uk/data_request/cif. Supplementary data associated with this article can be found, in the online version, at http://dx.doi.org/10.1016/j.ica.2015.07.024.

References

[1] A. Scozzafava, T. Owa, A. Mastrolorenzo, C.T. Supuran, Curr. Med. Chem. 10 (2003) 925.
[2] R.B. Silverman, The Organic Chemistry of Drug Design and Drug Action, Academic Press, New York, 1992.
[3] T. Nogrady, Medicinal Chemistry, 2° ed., Oxford University Press, Oxford, 1988.
[4] T. Owa, H. Yoshino, T. Okauchi, K. Yoshimatsu, Y. Ozawa, N. Hata, J. Med. Chem. 42 (1999) 3789.
[5] A.E. Boyd, Diabetes 37 (1988) 847.
[6] C.T. Supuran, A. Scozzafava, A. Jitianu, Met. -Based Drugs 4 (1997) 307.
[7] C.W. Thornber, Chem. Soc. Rev. 8 (1979) 563.
[8] R.C. Ogden, C.W. Flexner, Protease Inhibitors in AIDS Therapy, Marcel Dekker, New York, 2001.
[9] C.T. Supuran, A. Scozzafava, A. Mastrolorenzo, Expert Opin. Ther. Pat. 111 (1999) 221.
[10] X. Guo, J. Li, F. Yang, J. Yang, D. Yin, Sci. Total Environ. 493 (2014) 626.
[11] J.W. Costerton, Z. Lewandowski, D.E. Caldwell, D.R. Korber, H.M. Lappin-Scott, Annu. Rev. Microbiol. 49 (1995) 711.
[12] P.S. Stewart, J.W. Costerton, *Lancet* 358 (9276) (2001) 135.
[13] S.J. Projan, P.J. Youngman, Curr. Opin. Microbiol. 5 (2002) 463.
[14] Z.H. Chohan, Transition Met. Chem. 34 (2009) 153.
[15] N.C. Baenziger, A.W. Struss, Inorg. Chem. 15 (1976) 1807.
[16] N. Absar, H. Daneshvar, G. Beall, J. Allergy Clin. Immunol. 96 (1994) 1001.
[17] J.H. Bormio Nunes, R.E. Ferraz de Paiva, A. Cuin, W.R. Lustri, P.P. Corbi, Polyhedron 85 (2015) 437.
[18] G. Karthikeyan, K. Mohanraj, K.P. Elango, K. Girishkumar, Russ. J. Coord. Chem. 32 (2006) 380.
[19] E. Schulz Lang, L.L. Marques, G. Manzoni de Oliveira, Z. Naturforsch. 60b (2005) 1264.
[20] L.L. Marques, G. Manzoni de Oliveira, E. Schulz Lang, Z. Anorg. Allg. Chem. 632 (2006) 2310.
[21] L.L. Marques, E. Schulz, Z. Anorg. Allg. Chem. 631 (2005) 745.
[22] L.L. Marques, G. Manzoni de Oliveira, E. Schulz, M.M. Anrakude Campos, L.R. Soccol Gris, Inorg. Chem. Commun. 10 (2007) 1083.
[23] M. Mondelli, F. Pavan, P.C. de Souza, C.Q. Leite, J. Ellena, O.R. Nascimento, G. Facchin, M.H. Torre, J. Mol. Struct. 1036 (2013) 180.
[24] A. García-Raso, J.J. Fiol, S. Rigo, A. Lópes-López, E. Molins, E. Espinosa, E. Borrás, G. Alzuet, J. Borrás, A. Castiñeiras, Polyhedron 19 (2000) 991.
[25] B. Kesimli, A. Topacli, Spectrochim. Acta A 57 (2001) 1031.
[26] G. Kanagaraj, G.N. Rao, Synth. React. Inorg. Met.-Org. Chem. 22 (1992) 559.
[27] CrysAlisPro, Oxford Diffraction Ltd., version 1.171.33.48 (release 15–09-2009 CrysAlis171.NET).
[28] G.M. Sheldrick, Acta Crystallogr. A 64 (2008) 112.
[29] G.A. O' Toole, R. Kolter, Mol. Microbiol. 28 (1998) 449.
[30] L.J. Farrugia, J. Appl. Crystallogr. 30 (1997) 565.
[31] M.H. Torre, S. Calvo, H. Párdo, A.W. Mombru, J. Coord. Chem. 58 (2005) 513.
[32] F. Blasco, L. Perelló, J. Latorre, J. Borrás, S. García-Granda, J. Inorg. Biochem. 61 (1996) 143.
[33] W.L. Driessen, P.H. Van der Voort, Inorg. Chim. Acta 21 (1977) 217.
[34] B.D. Corbin, E.H. Seeley, A. Raab, J. Feldmann, M.R. Miller, V.J. Torres, K.L. Anderson, B.M. Dattilo, P.M. Dunman, R. Gerads, Science 319 (2008) 962.
[35] M.J. Horsburgh, S.J. Wharton, M. Karavolos, S.J. Foster, Trends Microbiol. 10 (2002) 496.
[36] B.S. Creaven, D.A. Egan, D. Karcz, K. Kavanagh, M. McCann, M. Mahon, A. Noble, B. Thati, M. Walsh, J. Inorg. Biochem. 101 (2007) 1108.
[37] X. Xiang-Jiao, X. Zhi, Q. Zu-De, H. An-Xin, L. Chao-Hong, L. Yi, Thermochim. Acta 476 (2008) 33.
[38] A.A. Nejo, G.A. Kolawole, M.C. Dumbele, A.R. Opoku, J. Coord. Chem. 63 (2010) 4367.
[39] N. Raman, V. Muthuraj, S. Ravichandran, A. Kulandaisamy, Poc. Indian Acad. Sci. 115 (2003) 161.
[40] Z.H. Chohan, M.S. Iqbal, S.K. Aftab, A. Rauf, J. Enzym. Inhib. 27 (2012) 223.
[41] Y. Ma, Y. Xu, B.D. Yestrepsky, R.J. Sorenson, M. Chen, S.D. Larsen, H. Sun, Plosone 7 (2012) e47255.
[42] D.B. Wunder, V.A. Bosscher, R.C. Cok, R.M. Hozalski, Water Res. 45 (2011) 2270.
[43] J.M. Patti, M. Hook, Curr. Opin. Cell Biol. 6 (5) (1994) 752.
[44] P.E. Kolenbrander, R.N. Andersen, R.A. Baker, H.F. Jenkinson, J. Bacteriol. 180 (1998) 290.